Controlled Directional Growth of TiO2 Nanotubes

In, Su-il; Hou, Yidong; Abrams, Billie; Vesborg, Peter Christian Kjærgaard; Chorkendorff, Ib

Published in:
Journal of The Electrochemical Society

Link to article, DOI:
10.1149/1.3308599

Publication date:
2010

Document Version
Publisher's PDF, also known as Version of record

Journal of The Electrochemical Society, **157** (5) E69-E74 (2010)
0013-4651/2010/157(5)/E69/6/$28.00 © The Electrochemical Society

Controlled Directional Growth of TiO_2 Nanotubes

Su-Il In, Yidong Hou, Billie L. Abrams, Peter C. K. Vesborg, and Ib Chorkendorff[*,z]

Center for Individual Nanoparticle Functionality, Department of Physics, Technical University of Denmark, 2800 Kongens Lyngby, Denmark

We demonstrate how the anodization direction and growth rate of vertically aligned, highly ordered TiO_2 nanotube (NT) arrays can be controlled and manipulated by the local concentration of O_2 in the electrolyte. This leads to the growth of highly active TiO_2 NT arrays directly on nonconducting substrates in a single step. By controlling the oxygen concentration, the electrical contact to the titanium film can be preserved until the entire film is anodized. This approach to growing transparent TiO_2 NT films yields possibilities for using glass without any transparent conducting oxide coating as substrates. The role of molecular oxygen on the anodization and the means necessary for controlling the growth direction were investigated through the use of labeled oxygen and concentration gradient experiments.
 [DOI: 10.1149/1.3308599]

Manuscript received December 10, 2009. Published March 15, 2010.

Highly ordered, large-aspect ratio TiO_2 nanotubes (NTs)[1-7] offer possibilities in the area of sustainable energy due to enhanced photocatalytic water-splitting activity[2,8] and applications in solar cells.[9-12] This is because they allow for fast separation of electron–hole pairs, while at the same time, they expose a high surface area where photocatalytic reactions take place. Another important use is in self-cleaning or environmental remediation technology where TiO_2 NTs may have a high activity for photo-oxidation of organics.[13,14] Specifically, the formation of optically transparent TiO_2 NTs onto nonconducting substrates allows access to new photocatalytic environments, i.e., gas-phase photocatalysis using glass, polymer, or ceramic substrates. Here, we demonstrate how the growth direction and rate of these NT arrays can be controlled by the local O_2 concentration allowing a single-step growth of TiO_2 NT directly onto nonconducting substrates.

Generally, planar TiO_2 films can be prepared using the sol–gel method[15,16] or by sputtering (either dc or radio frequency),[17,18] resulting in reasonably reactive surface areas. Attempts to enhance the surface area of TiO_2 have been explored by synthesizing TiO_2 NTs using a template process.[19,20] Recently, vertically oriented, highly ordered TiO_2 NT array thin films made by anodization of titanium metal have received much attention because of their high surface area nanostructure.[2,6,7,21] The anodization of Ti using a fluoride-containing polyhydric alcohol such as ethylene glycol (EG) as the electrolyte results in ordered TiO_2 NT arrays.[22,23] The anodization process depends critically on pH, F^- concentration, temperature, and EG and water concentrations.[22-24] Various mechanisms have been proposed to account for the TiO_2 NT forming,[23,25] but the roles of the individual experimental parameters are not completely understood.

It has been reported that the anodization of single-layer titanium films onto nonconducting glass substrates is not possible as the metal layer in contact with the electrolyte surface is rapidly etched away, as shown in Fig. 1a.[21] Mor et al. reported that this problem may be circumvented by a two-step process or "bilayer" approach, which involves anodization down to a thin "first layer" of Ti metal, so that the electrical contact is not broken.[21] This first thin Ti layer is subsequently oxidized thermally, leading to a transparent TiO_2 NT film on top of a conventional TiO_2 thin film. This approach does produce TiO_2 NTs onto nonconducting substrates but involves a multistep approach, and there is a dense oxide film between the support and the NT layer.[21] The method presented here, which involves controlling the NT array growth direction through the molecular oxygen concentration, also alleviates the contact-loss problem by ensuring that the contact point is the last part (Fig. 1b) to be anodized, a principle that may also be used for other anodization processes as well. This approach also allows for the formation of the TiO_2 NTs onto a nonconducting substrate in a one-step process where the NTs are in direct contact with the truly nonconducting (i.e., Pyrex glass) substrate.

Experimental

Formation of TiO_2 NTs.— The substrate was Pyrex glass coated with thermally deposited metallic titanium. First, a titanium film (400 nm thick) was deposited on 4 in. Pyrex wafers (JINSOL) via E-beam deposition (Wordentec QCL800). Before the Ti film deposition, the Pyrex wafers were cleaned using sulfuric acid with ammonium peroxydisulfate at 80°C for 10 min, rinsed with water for 10 min, and dried at 250°C overnight. The purity of the Ti target used was 99.995%. The base chamber pressure was approximately 5×10^{-7} mbar. The deposition rate was 10 Å/s. Before the anodization, the titanium metal film was cleaned with acetone and ethanol, followed by a deionized water rinse. The anodization was performed using a two-electrode cell with titanium deposited on Pyrex as the working electrode and carbon paper as the counter electrode. Anodizations were carried out for about 1.5 h at a constant applied voltage of 10 V at room temperature in an electrolyte mixture of 0.3 wt % NH_4F (98%, ACS reagent, Sigma-Aldrich) and 2 vol % H_2O in EG (ReagentPlus, ≥99%, Aldrich). Figure S1 of supplementary materials[26] (from SOM) shows the experimental setup used in this work. As expected, there was no significant ohmic drop across the sample at any time during the process because the sheet resistance of the film was ~1 Ω/□ and the peak anodic current was less than about 0.5 mA (see Fig. S2 of supplementary materials[26]). The temperature of the electrolyte solution was 298 K. To convert the amorphous TiO_2 NT array film into anatase, the as-prepared sample was annealed at 450°C for 2 h in air (30 mL/min).

Measurement of oxygen concentrations in solution.— The dissolved oxygen present in the electrolyte during the anodization was monitored by an OxySense 210 T noninvasive oxygen determination instrument. This technique utilized the effect of oxygen on the fluorescence lifetime of a ruthenium (Ru) complex that was excited by a blue light-emitting diode with a wavelength between 400 and 500 nm. The Ru complex was immobilized in a stable polymer and placed in the form of a 5 mm diameter dot on the inner wall of the container submerged in the electrolyte in the same depth as the sample being anodized and 20 mm from the sample. The excitation light source/detector was placed outside the container but within a 5 mm distance of the dot to measure the O_2 concentration. We noticed that the oxygen diffusion was somewhat higher than what would be expected for a standard diffusion constant of $D_{O_2} = 1.97 \times 10^{-5}$ cm^{-2}/s. This was ascribed to the nonideal conditions under

* Electrochemical Society Active Member.
z E-mail: ibchork@fysik.dtu.dk

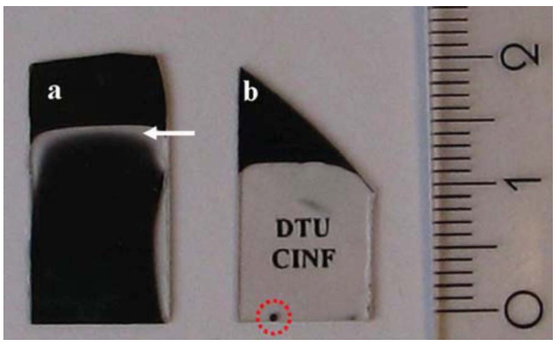

Figure 1. (Color online) A digital photograph showing (a) unsuccessful anodization of single-layer Ti film onto a nonconducting glass substrate (white arrow points out rapidly etched part consequently, causing electric disconnection) and (b) successful direct anodization of single-layer Ti film onto a nonconducting glass substrate by a bottom contact method (black letters are clear and the bottom contact point remains metallic).

which these experiments were performed for measuring diffusion and was not pursued further as the establishment of a strong gradient in the oxygen concentration was successful.

Oxygen isotope labeling experiment: SIMS.— The ion probe analysis was performed at Danchip, DTU, using a quadrupole ATOMIKA 4000 secondary-ion mass spectrometry (SIMS) instrument. Sputter etching of the surface was accomplished with 5 keV Cs^+ ions raster scanned over 300 μm (I = 10 nA) at 20° impact angle from normal incidence. The main chamber base pressure was about 10^{-10} Torr. Oxygen isotopes were analyzed as O^- ions produced by a bombardment by a Cs^+ primary beam (10 nA intensity) of around 15 μm diameter. The oxygen isotopes were subsequently measured in a single channeltron plate.

UV/visible measurements.— UV/visible spectra were collected using a Cary 1e spectrophotometer operated in a dual beam mode and with an uncoated Pyrex sample in the reference beam.

Photocatalytic activity.— The photocatalytic oxidation of acetone over TiO_2 thin films was performed in a 440 mL steel reactor with a quartz window at ambient temperature. A circulating gas pump was set up between the reactor and gas chromatograph [Perkin Elmer Clarus 500, Porapak QS 80/100 mesh, 2 m × 0.125 in.]. A 4 in. diameter Pyrex wafer coated with TiO_2 NTs was placed in the reactor. Liquid acetone (1 μL) was injected into the reactor. Inside the reactor, the acetone vaporized and was allowed to reach adsorption equilibrium with the catalyst in the reactor before an experiment. The initial concentration of acetone after the adsorption equilibrium was about 720 ± 20 ppmv. A 4 W UV lamp (UVP UVGL-15) with a dominant emission at 345–365 nm was used as an excitation light source. Figure S6 of supplementary materials[26] shows the UV light source spectrum. Integrated UV intensity measured with a UV radiometer was 1.75 mW/cm^2.

Results and Discussion

The realization that molecular oxygen enhances the anodization process makes it important to establish well-defined oxygen concentration gradients in the electrolyte. The oxygen concentration profile can be established in numerous ways, but here, we shall highlight two approaches in detail: the "bottom contact" method and the "auxiliary anode" method.

Bottom contact method.— In the bottom contact method, the entire closed system containing the electrolyte, headspace, and anode is first deaerated with argon. The anode is then submerged into the electrolyte, mounted vertically with the electrical contact to the Ti layer at the largest possible distance from the surface, as shown in the diagram of Fig. 2. After the electrolyte is saturated with Ar, the headspace is exchanged with atmospheric air and the anodization process is initiated.

In this manner, an oxygen concentration gradient is established in the electrolyte being highest at the surface, which is in contact with air. Figure 2a-c shows the process of forming the NT arrays in this manner, where the anodization was stopped after 3760 s, i.e., when the top part of the sample is getting transparent, but before the entire Ti film (400 nm) is completely converted into NT, which for this type of sample usually takes ~4400 s. Cross-sectional scanning electron microscopy (SEM) images of a sample were taken from each part of the anode corresponding to 1, 2, and 3 cm below the electrolyte surface, respectively. Figure 2a shows the fully anodized upper part of the anode where there is no Ti metal layer remaining. Figure 2b is the middle part of the anode, which still has some Ti metal layer remaining (~30 nm), and Fig. 2c shows the bottom part of the anode, which has more Ti metal layer left (~50 nm). Typically, we start with a Ti metal layer, 400 nm in thickness, which

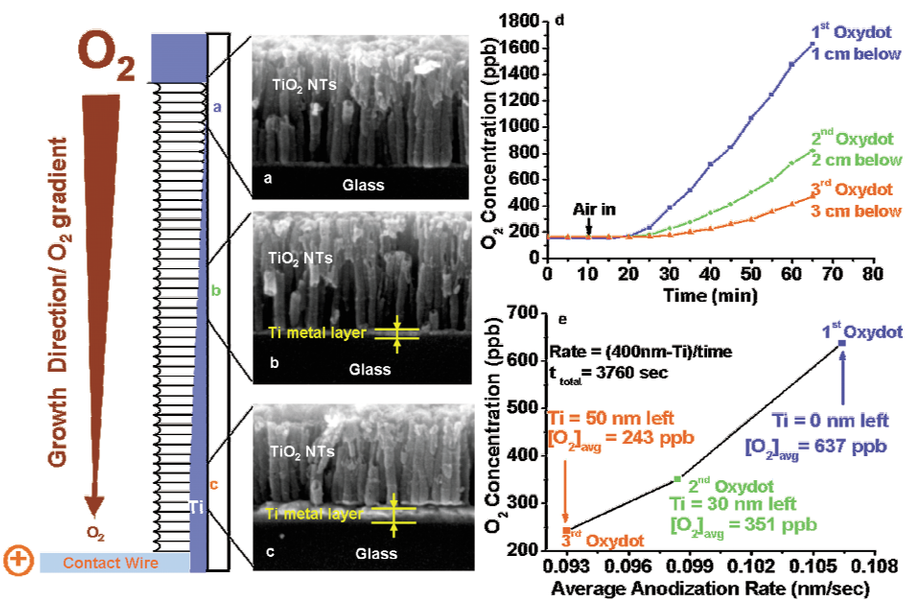

Figure 2. (Color online) Schematic diagram and corresponding SEM image of bottom contact method of anodization process generating a 400 nm thick TiO_2 NT array thin film. The big arrow (dark red) shows the direction forming TiO_2 NTs as a result of the enhanced anodization rate. The enhanced rate is due to higher oxygen concentration at the top. SEMs were taken at 1, 2, and 3 cm depths at different stages of the anodization process. (a) The corresponding SEM image at 1 cm shows no Ti metal, remaining consistent with this part being transparent, i.e., completely anodized. (b) At 2 cm, the presence of a thin Ti metal layer is indicated by the (yellow) arrows between the TiO_2 NTs and the glass substrates. (c) Near the contact point (3 cm) resides the thickest Ti metal layer remaining because it is the last region to be fully converted to NTs. (d) O_2 concentration as a function of time for each position of the SEM images. (e) Average anodization rate at various average oxygen concentrations corresponding to the SEM images of parts a, b, and c.

usually leads to an NT layer of about the same length, accompanied by a variable volume expansion on the order of 1–1.2. This expansion is somewhat less than what has previously been reported.[27,28] The NTs shown in this work have tube lengths of about 400 nm with an outside diameter of ~30 nm and an inside diameter of ~20 nm. We have also used the bottom contact method successfully to grow films up to 1000 nm thick. Viewed from the side, the NT samples look thin and elongated; from the top, they are hollow and highly ordered.

The oxygen concentrations were measured with an oxygen sensor (OxySense). Three Oxydots were mounted on the inside of the container in the electrolyte at depths corresponding to the SEM locations. The oxygen concentration profiles, as a function of time for each portion of the TiO_2 NT film, are plotted in Fig. 2d.

Initially, the system was deaerated by purging N60 argon until the oxygen concentration reading by the three Oxydots, each corrected for their individual offsets, gave constant readings corresponding to the detection limit (<0.18% of saturation). Oxydots monitor oxygen diffusion to the different portions of the sample during anodization. Figure 2e is the measured anodization rate extracted from Fig. 2a-c vs the average oxygen concentration at each position. It is observed that the rate increases with increasing oxygen concentration, although the enhancement due to oxygen is modest. Performing the same experiments without oxygen above the electrolyte or a saturated electrolyte in contact with air would lead to random initiations of the anodization and usually premature loss of contact. Because oxygen obviously enhances the anodization process, the NT formation can be controlled to proceed from the top toward the bottom contact with no loss of contact.

Auxiliary anode method.— In the auxiliary anode method, it is also possible to verify the significance of oxygen for the TiO_2 NT growth without using air and without growing the film from the liquid/air interface down. For example, a localized source of oxygen can be established by electrolysis on a gold wire under the anode in a deaerated container. It is not desired to have oxygen bubbling uncontrollably, but rather to have bubbles adhering to the wire and acting as a diffusion source of oxygen.

If +5 V is applied to the Au wire (with respect to a carbon paper counter electrode) until small oxygen bubbles cover the Au wire, as indicated in Fig. 3a, an oxygen gradient away from the Au wire will develop. In this case, the growth direction can be manipulated to be from the bottom toward the contact point at the top. I.e., the film grows toward the surface, opposite the bottom contact growth direction but still away from the O_2 source (Fig. 3a). Other geometries (i.e., horizontal) and sources of oxygen (i.e., air tubes) have been performed, all clearly demonstrating that the directional growth can be manipulated by the oxygen concentration (see Fig. 3b, where the Au wire (auxiliary anode) is placed at one end of the anode, opposite to the contact side).

Numerous other configurations were tested consistently, demonstrating that the process can be controlled by the oxygen gradient. Figure 4 shows a series of anodization configurations where the position of the anode has been altered with respect to the counter electrode as well as the electrolyte surface. However, in each case, one aspect is consistent; the contact point is farthest away from the O_2 source. In these figures, the black lines represent the counter electrode, the gray (red online) lines represent the Ti film, and the hollow lines represent the Pyrex glass substrate. The dark dots are due to the electrical contact points; the dark areas opposite these dots are due to the sample clamp. Finally, there are some areas where shadows can be seen, which could be due to convection in the electrolyte, but this phenomenon is not yet completely understood. Along with these configurations, we have grown transparent TiO_2 NT films directly on Pyrex wafers up to a 4 in. diameter using O_2 gradients to prevent premature loss of contact. This demonstrated the scalability of the method.

In all cases, it is crucial to avoid oxygen evolution near the contact point itself, which is at +10 V, because that would enhance the anodization locally, leading to premature loss of contact. Thus, the choice of wire material used to make electrical contact is important. It must consist of self-passivating materials such as Ti or Al,

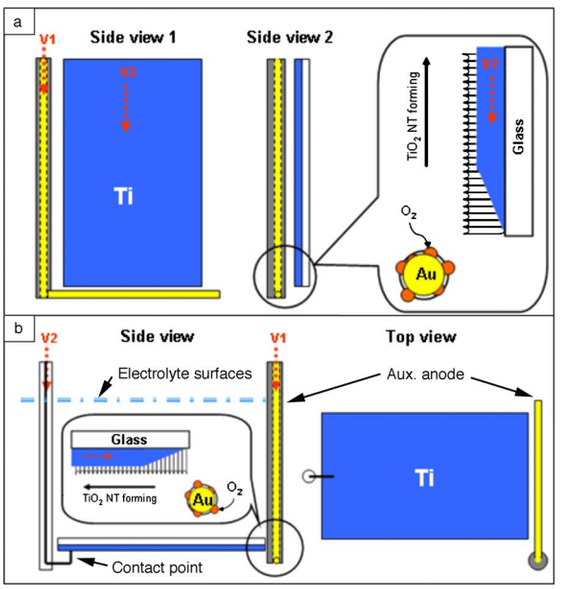

Figure 3. (Color online) Schematic diagrams of the experimental set-ups used for growing TiO_2 NT array films by controlling oxygen concentration. (a) A voltage V1 of 5 V is applied to the Au wire until oxygen covers the Au wire, and then 10 V is applied to V2 from the top of the anode. (b) The anode is placed horizontally under the electrolyte solution. At the point furthest away from the Au wire, 10 V is applied to V2. Both principles have been demonstrated successfully.

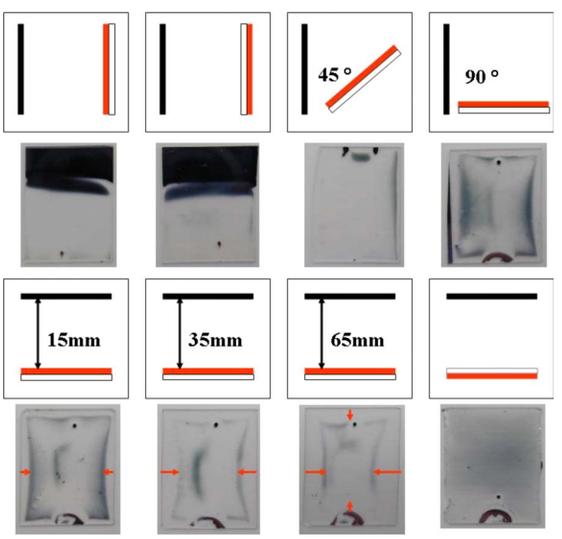

Figure 4. (Color online) Various anodization configurations showing that on a truly nonconducting substrate, TiO_2 NTs can be grown in a single step as long as the contact is at the furthest distance from the electrical contact point. In the diagrams, the black lines represent the counter electrode, the gray (red) lines represent the Ti film, and the hollow lines represent the Pyrex glass substrate. Under each diagram is a photograph of the TiO_2 NT film after anodization. The small dark dots represent the position of the contact point. The darker dots opposite the contact point represent the position where the sample holder was in place. Also, there is some shadowing on some of the samples depending on the configuration possibly due to convection in the electrolyte.

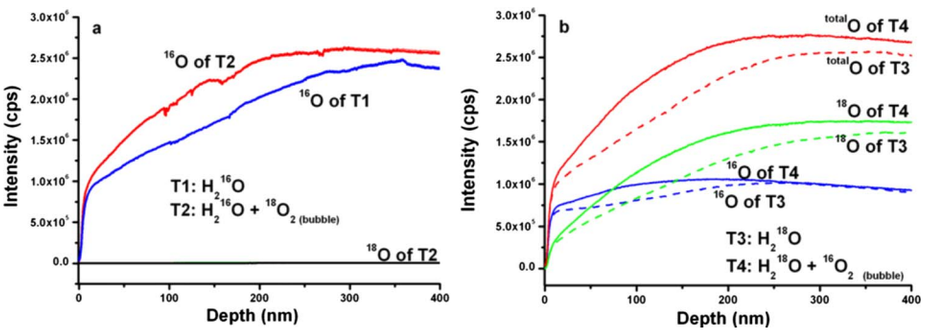

Figure 5. (Color online) (a) SIMS data showing oxygen depth profiles of TiO_2 NTs prepared with isotopically labeled molecular oxygen. T1 is without labeled O_2 (the control, blue line). T2 is the experiment utilizing ^{18}O-labeled O_2 bubble held near the anode (red and black lines). The total oxygen flux in both cases is similar to ^{16}O flux from TiO_2 NTs. ^{18}O is negligible. (b) SIMS data showing depth profiles of TiO_2 NTs of isotope-labeled water experiment. The solid lines represent labeled water with $^{16}O_2$ bubble present. The dotted lines represent experiments without $^{16}O_2$ bubble present. The upper (red) lines represent the total oxygen flux, the second set of (green) lines represent the ^{18}O flux, and the third set of (blue) lines represent the ^{16}O flux from TiO_2 NT growth.

suppressing oxygen evolution, while oxygen-evolving materials such as gold (Au) or platinum (Pt) must be excluded.

To elucidate the mechanism experimentally, we used ^{18}O-isotope-labeled molecular oxygen and water to trace the oxygen location and determine its role in the NT formation. Two different samples were prepared in a (initially) deaerated electrolyte, T1: 2 vol % of H_2O (standard electrolyte) and T2: 2 vol % of H_2O with a bubble of ^{18}O-labeled O_2 held near the anode. The T1 sample constitutes the reference sample and only displays the ^{16}O isotope (Fig. 5a, blue (T1) line). When an ^{18}O-labeled oxygen bubble is suspended near the anode (T2) during anodization, ^{18}O remains absent in the depth profile (Fig. 5a, black (bottom T2) line). We do, however, see an increased ^{16}O signal in the SIMS profile (Fig. 5a, red (top T2) line). The enhanced SIMS signal could be due to a geometric effect in the SIMS measurement. For example, if the NTs grown under the influence of O_2 that have slightly different geometries (i.e., wall thickness/diameter ratio) than those grown without O_2, the oxygen ion yield would be affected. Similar effects are observed when the ^{16}O bubble was provided near the anode (T4, see Fig. 5b). From this, it is concluded that oxygen from O_2 is not implemented in TiO_2 in measurable amounts.

Beyond the experiment shown in Fig. 5a, showing that no detectable $^{18}O_2$ was implemented in the TiO_2 NT, we also performed experiments using ^{18}O-labeled water (samples T3 and T4). These samples were prepared like T1 and T2 but with the following modifications: T3: 2 vol % of ^{18}O-labeled $H_2{}^{18}O$ and T4: 2 vol % of ^{18}O-labeled $H_2{}^{18}O$ and an unlabeled O_2 bubble near the anode. In this case, both ^{16}O and ^{18}O were clearly present in the film (Fig. 5b). Given the isotopic purity of the labeled water (>97% ^{18}O, CK Gas Products Ltd.) and size of the ^{16}O signal, there can be no doubt that the oxygen from EG is also being incorporated into the TiO_2 NTs as there is no other source of ^{16}O present. It has been considered that water is the main oxygen source in forming TiO_2 NTs,[25] but the availability of oxygen from organic solutions has also been suggested.[23] The current data also provide experimental support that EG does indeed donate oxygen to the NT structures. From this result (Fig. 5b), it seems that water and EG could be acting as competing oxygen sources during anodization with EG leading in the very beginning. But eventually, the dominant oxygen contribution is from water despite the ~16:1 molar ratio of EG to water. We believe that the mass transport of reactants down through the growing film (of high aspect ratio NTs) may account for this because the smaller water molecules are likely to diffuse faster than EG.

To explain how O_2 enhances the anodization without being implemented in the oxide, we propose the mechanism illustrated in Fig. 6. The model is based on the following two assumptions: (*i*) that oxygen vacancies form at the electrolyte surface interface above some critical breakdown field strength across the oxide (Fig. 6a), a phenomenon also reported by Zhang et al.[29] and generally accepted for anodization of Al and Ti,[30,31] (*ii*) and that this vacancy (e.g., due to steric hindrance) cannot accommodate a water molecule but can accommodate an O_2 molecule (Fig. 6b). Using these assumptions, we suggest that a partial oxidation of the adsorbed O_2 molecule by the strongly anodic-biased oxide can occur. This yields an electrostatic attractive force between the outermost O-atom of the adsorbed molecule and anions or dipoles in the surroundings. Fluoride ions cannot readily donate electrons, but water molecules (or potentially hydroxyl ions) can. Figure 6c and d illustrates the process where the H-atoms of a water molecule donate electrons to the surface via the adsorbed oxygen, effectively filling the surface vacancy and liberat-

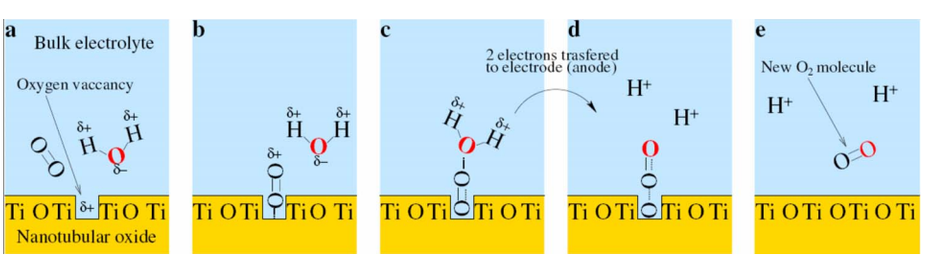

Figure 6. (Color online) Autocatalytic mechanism for O_2 anodization enhancement. (a) Initial situation where the strong anodic bias has created an oxygen vacancy at the surface. (b) O_2 is adsorbed in the vacancy. (c) Electrostatic attraction between the adsorbed O_2 molecule attracts a (polar) water molecule. (d) The H atoms of the water molecule are oxidized via the adsorbed O_2 molecule, and the donated electrons give rise to the anodization current. (e) The O atom from the water molecule covalently bonds to the outer O atom of the adsorbed O_2 molecule, causing a scission of the original O–O bond, leaving the vacancy annihilated and forming a (new) O_2 closing the cycle.

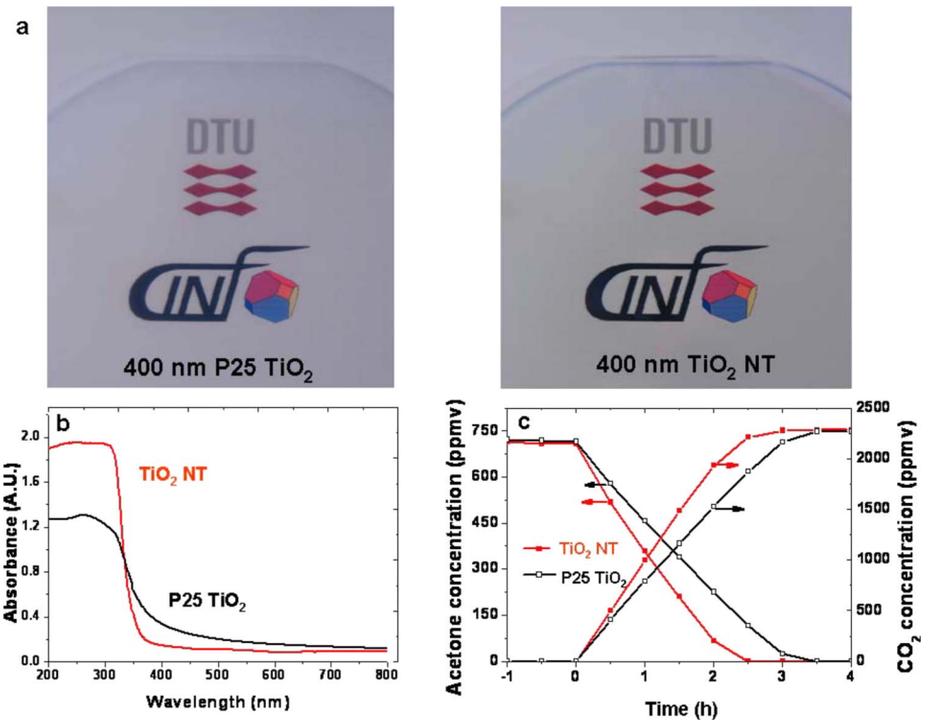

Figure 7. (Color online) Activity and absorbance measurements comparing TiO_2 NTs and P25 TiO_2 for the same thickness (400 nm) on a Pyrex glass substrate. (a) Left: Spin-coated P25 TiO_2 on a 4 in. Pyrex wafer (see Fig. S7 of supplementary materials[26] for SEM). Right: Transparent TiO_2 NTs formed on the 4 in. Pyrex wafer. (b) Optical absorbance spectra of TiO_2 NTs red curve and P25 TiO_2 black line. (c) Photocatalytic activity measurements comparing TiO_2 NTs to P25 TiO_2. Changes in acetone (left axis) and CO_2 concentrations (right axis) are plotted as a function of time in the presence of a TiO_2 NT array film red lines, filled boxes and a P25 thin film black line, open boxes under UV irradiation.

ing a new O_2 molecule (Fig. 6e). The net (anodic) reaction in this case remains

$$TiO + H_2O(+ O_2) \rightarrow TiO_2 + 2H^+(+ O_2) + 2e^- \quad [1]$$

This is in accordance with the generally accepted picture in the literature of water acting as the main oxygen source.[3] In an isotope-labeled experiment using an ^{18}O-labeled suspended bubble to initiate the anodization (i.e., experiment T2 above), one would expect that near the very top of the NTs corresponding to initial growth, there should be an enrichment of ^{18}O in the film. The reason may be seen in Fig. 6b, where we find that the oxygen atom filling the vacancy comes from the O_2 molecule, and as such, has a probability of donating an ^{18}O atom of $p = 2^{-n}$, where n is the number of times the molecule has previously catalyzed the reaction. Within the sensitivity of our SIMS data, we do not see such an initial hump in the ^{18}O signal in the T2 profile. This is, however, expected because the total expected ^{18}O amount only should be about 1 monolayer to begin with; furthermore, chemical dissolution of the NTs during growth mostly etches the top of the tubes, whereby the labeled oxygen is lost.

To demonstrate that such NT growth on insulating material has the desired optical properties and catalytic activity (400 nm), we measured the absorbance and photocatalytic activity of the TiO_2 NTs. They were grown on 4 in. Pyrex wafers and compared to P25 TiO_2 spin-coated on similar wafers with similar thickness, as shown in Fig. 7a. As-anodized TiO_2 NTs were amorphous and were thus annealed at 450°C to convert them to anatase [see X-ray diffraction and X-ray photoemission spectroscopy (XPS) data in Fig. S3 and S4 of supplementary materials,[26] respectively]. The absorbance spectra of annealed TiO_2 NT array films were compared with those of the same thickness of the P25 TiO_2-coated films. The data of Fig. 7b clearly show that the NT films are much more transparent over the entire visible spectrum relative to the P25 TiO_2 powder, because the latter exhibits a much higher scattering loss and therefore has a dull gray appearance, as seen in the photographs in Fig. 7a.

The photocatalytic activity was evaluated by the oxidation of gaseous acetone under UV light irradiation (see Fig. S5 of supplementary materials[26]) utilizing a batch reactor with principles of operation similar to that described by Yu et al.[32,33] Here, however, a GC was used to evaluate the evolution of any possible organic intermediates. Figure 7c shows the acetone concentration and the subsequently evolved CO_2 as a function of time. Apart from the decay of the acetone, only the final products for complete mineralization of acetone, CO_2, was observed in an almost stoichiometric ratio 1:3. The photocatalytic activity for acetone degradation over the TiO_2 NT film (318 ppmv/h, corresponding to $\sim 1.04 \times 10^{15}$ acetone molecules/s) at least as good as the commercial 400 nm thick P25 TiO_2 for similar conditions (see Fig. S6 of supplementary materials[26]).

Conclusion

In this work, we show that it is possible to control the growth rate and thus the direction of TiO_2 NT arrays by manipulating the oxygen concentration gradient. This has the advantage that such NTs can be grown from a metallic titanium film deposited on an insulating material in a one-step procedure over large areas (>4 in. wafer). We demonstrate that the NT arrays made in this manner maintain the desired properties concerning mineralization of organic compounds for self-cleaning purposes and optical properties, i.e., transparency. The procedure described here is versatile and promising for a large-scale production of transparent NT arrays on insulating media, an effect that may also be pursued for anodization of other materials. An autocatalytic model was proposed based on the fact that labeled oxygen, ^{18}O, is not incorporated in the NT array (as judged by SIMS analysis) showing that O_2 does not act as the primary source of oxygen. It is, however, found that the oxygen from the labeled water is incorporated in the NTs in competition with oxygen from EG.

Acknowledgment

We thank John Larsen for his help in XPS experiments. The Center for Integrated Nanoparticle Functionality is funded by the National Danish Research Council. This work was also funded by the Clean Catalytic Surfaces project through the Danish Innovations consortium.

Technical University of Denmark assisted in meeting the publication costs of this article.

References

1. D. Gong, C. A. Grimes, O. K. Varghese, W. C. Hu, R. S. Singh, Z. Chen, and E. C. Dickey, *J. Mater. Res.*, **16**, 3331 (2001).
2. C. A. Grimes, *J. Mater. Chem.*, **17**, 1451 (2007).
3. G. K. Mor, O. K. Varghese, M. Paulose, K. Shankar, and C. A. Grimes, *Sol. Energy Mater. Sol. Cells*, **90**, 2011 (2006).
4. O. K. Varghese, D. W. Gong, M. Paulose, C. A. Grimes, and E. C. Dickey, *J. Mater. Res.*, **18**, 156 (2003).
5. O. K. Varghese, D. W. Gong, M. Paulose, K. G. Ong, E. C. Dickey, and C. A. Grimes, *Adv. Mater.*, **15**, 624 (2003).
6. V. Zwilling, M. Aucouturier, and E. Darque-Ceretti, *Electrochim. Acta*, **45**, 921 (1999).
7. V. Zwilling, E. Darque-Ceretti, A. Boutry-Forveille, D. David, M. Y. Perrin, and M. Aucouturier, *Surf. Interface Anal.*, **27**, 629 (1999).
8. G. K. Mor, K. Shankar, M. Paulose, O. K. Varghese, and C. A. Grimes, *Nano Lett.*, **5**, 191 (2005).
9. M. Grätzel, *Nature (London)*, **421**, 586 (2003).
10. J. R. Jennings, A. Ghicov, L. M. Peter, P. Schmuki, and A. B. Walker, *J. Am. Chem. Soc.*, **130**, 13364 (2008).
11. T. S. Kang, A. P. Smith, B. E. Taylor, and M. F. Durstock, *Nano Lett.*, **9**, 601 (2009).
12. K. Lee, S. W. Park, M. J. Ko, K. Kim, and N.-G. Park, *Nature Mater.*, **8**, 665 (2009).
13. Z. Liu, X. Zhang, S. Nishimoto, M. Jin, D. A. Tryk, T. Murakami, and A. Fujishima, *J. Phys. Chem. C*, **112**, 253 (2008).
14. Z. Y. Liu, X. T. Zhang, S. Nishimoto, T. Murakami, and A. Fujishima, *Environ. Sci. Technol.*, **42**, 8547 (2008).
15. J. Medina-Valtierra, J. Garcia-Servin, C. Frausto-Reyes, and S. Calixto, *Appl. Surf. Sci.*, **252**, 3600 (2006).
16. Y. F. Zhu, L. Zhang, W. Q. Yao, and L. L. Cao, *Appl. Surf. Sci.*, **158**, 32 (2000).
17. A. Karuppasamy and A. Subrahmanyam, *J. Appl. Phys.*, **101**, 064318 (2007).
18. A. Mills, J. S. Wang, M. Crow, G. Taglioni, and L. Novella, *J. Photochem. Photobiol., A*, **187**, 370 (2007).
19. P. Hoyer, *Langmuir*, **12**, 1411 (1996).
20. P. Hoyer, *Adv. Mater.*, **8**, 857 (1996).
21. G. K. Mor, O. K. Varghese, M. Paulose, and C. A. Grimes, *Adv. Funct. Mater.*, **15**, 1291 (2005).
22. J. M. Macak and P. Schmuki, *Electrochim. Acta*, **52**, 1258 (2006).
23. K. S. Raja, T. Gandhi, and M. Misra, *Electrochem. Commun.*, **9**, 1069 (2007).
24. K. S. Raja, M. Misra, and K. Paramguru, *Electrochim. Acta*, **51**, 154 (2005).
25. J. M. Macak, H. Tsuchiya, A. Ghicov, K. Yasuda, R. Hahn, S. Bauer, and P. Schmuki, *Curr. Opin. Solid State Mater. Sci.*, **11**, 3 (2007).
26. See Supplementary Material at http://dx.doi.org/10.1149/1.3308599 E-JESOAN-157-087004 for additional information.
27. D. J. LeClere, A. Velota, P. Skeldon, G. E. Thompson, S. Berger, J. Kunze, P. Schmuki, H. Habazaki, and S. Nagata, *J. Electrochem. Soc.*, **155**, C487 (2008).
28. A. Valota, D. J. LeClere, T. Hashimoto, P. Skeldon, G. E. Thompson, S. Berger, J. Kunze, and P. Schmuki, *Nanotechnology*, **19**, 355701 (2008).
29. L. Zhang, D. D. Macdonald, E. Sikora, and J. Sikora, *J. Electrochem. Soc.*, **145**, 898 (1998).
30. S. J. Garcia-Vergara, P. Skeldon, G. E. Thompson, and H. Habazaki, *Electrochim. Acta*, **52**, 681 (2006).
31. F. Thébault, B. Vuillemin, R. Oltra, J. Kunze, A. Seyeux, and P. Schmuki, *Electrochem. Solid-State Lett.*, **12**, C5 (2009).
32. J. G. Yu, Y. R. Su, and B. Cheng, *Adv. Funct. Mater.*, **17**, 1984 (2007).
33. J. G. Yu, J. C. Yu, M. K. P. Leung, W. K. Ho, B. Cheng, X. J. Zhao, and J. C. Zhao, *J. Catal.*, **217**, 69 (2003).